Modulation of the acidity of a vermiculite and its potential use as a catalytic support

Jahaziel Amaya[a], Luis Bobadilla[b], Lola Azancot[b], Miguel Centeno[b], Sonia Moreno[a], and Rafael Molina[a]*.

[a] *Estado Sólido y Catálisis Ambiental (ESCA) Departamento de Química, Facultad de Ciencias, Universidad Nacional de Colombia, Kra 30 N°45-03 Bogotá Colombia.*
[b] *Instituto de Ciencia de Materiales de Sevilla, Centro mixto Universidad de Sevilla-CSIC, 49 Av. Américo Vespucio, 41092 Sevilla, España*
E-mail: ramolinag@unal.edu.co

Abstract

The modulation and characterization of the acidity of a vermiculite was carried out, which was modified by delamination by means of hydrothermal and acid treatments with the subsequent incorporation of AlZr and AlCe species to modulate the acidity. The effect of these species was evaluated regarding the structural (XRD, XPS and IR), textural (N_2 sortometry), and acidity properties (NH_3-TPD, NH_3-DRIFTS and CO adsorption at low temperature). The catalytic performance was studied in the dehydration-dehydrogenation reactions of 2-propanol and the hydro-conversion of decane, which generate important information about the acidity properties such as the type, number and strength of acidic sites. The correlation between the number, type and acid strength with the catalytic behavior allowed to establish the important effect regarding the nature of the mineral, its method of delamination and the nature of the incorporated cation, thus generating tools for controlled processes for the potentiation of the acidity of new supports from raw vermiculite.

Keywords: Delaminated vermiculite; acid modulator AlZr and AlCe; characterization of acidic properties; probe molecules; decane hydroconversion.

Introduction

Acid catalysts are used in different industrial processes such as: isomerization of olefins, dehydration of alcohols, Beckmann transitions, isomerization of paraffins, alkylation, cracking, dehydration, isomerization and alkylation [1] among many others, demonstrating the importance of this type of catalysis on an industrial level [2]. In this

context, the oil refining process has stimulated the search for solids with acid surface properties which are widely used in catalytic cracking, hydrocracking and hydro-isomerization processes [3].

The systematic study of clay minerals has been carried out for several decades given its natural origin, abundance, low cost and the processes of modification and potentiation of its environmentally friendly intrinsic acidity. Among the many uses for which it has been proposed is as an alternative for the development of acid supports or as catalysts for various applications, including use as an alternative to replace zeolites in catalytic processes [4].

Vermiculite in particular has attracted attention in acid catalysis due to its high interlayer charge attributed to the greater number of isomorphic substitutions of Si^{4+} for Al^{3+} in the tetrahedral layers compared with those present in montmorillonites [5]. This decompensation of layer charge generated by the isomorphic substitution described, promotes the formation of sites with an acid character, either because the deprotection of positive charges allows for the acceptance of electronic pairs (Lewis acidity) or because it can capture protons and then yield them (Brönsted acidity) [6]. However, the substitution of Si^{4+} ions for Al^{3+} ions leads to an excess of negative charge in the structure, which is compensated by Mg^{2+} or Ca^{2+}, which results in a poor swelling capacity [7], thus making it difficult to be modified in the interlayer. For the reduction of said excess layer charge, various processes of the natural mineral have been reported, such as HydroThermal Treatment (HTT) [8], the use of plasma [9], ultrasound [10], cationic or anionic surfactants, peroxide [9] or acid [11] or a combination of physical and chemical treatments, such as the use of peroxide with ultrasound [12]. These processes carried out on the raw vermiculite facilitate its subsequent structural modification. In this way, the mineral has been intercalated with organic surfactants [13], the sheets have been

exfoliated or opened (delamination) [11, 14] and, after employing HTT, the vermiculites have been modified with Zr and Ti species by a method of sulphation, generating more acidic sites in the material [15], or pillared with mixed oxides of Al-Zr, Al-Ce and Al-Hf, obtaining a catalytic performance similar or higher to catalysts based on USY zeolites in the decane reaction [6].

On the other hand, the use of probe molecules is a central tool in the determination of acidity in the solid state since it allows for obtaining specific information such as the number, type, strength and distribution of acid sites [16]. Accordingly, a large variety of probe molecules have been used, such as pyridine, trimethylphosphine oxide, carbon monoxide, quinoline and ammonia, among others, in order to determine and discriminate acid sites in the solid state [17]. Among these, ammonia is probably the most widely used in acidity measurements due to its strongly basic character, high thermal stability and its easy access to acidic sites in pores larger than 4 Å (3.7 x 3.9 x 3.1 Å) [18]. On the contrary, the adsorption of CO at a low temperature (-196 ºC) by FTIR has been less used in the characterization of clay minerals. It allows for obtaining useful information concerning the strength of the acid sites of the solids [19] and has not yet been reported to evaluate the acidity in vermiculites. On the other hand, catalytic reactions such as the dehydration of an alcohol and the hydro-conversion of decane generate important information not only regarding the catalytic performance but also concerning the acidic characteristics. In the first case, dehydration occurs in the acidic sites producing the corresponding alkene while acetone will be produced in the basic sites [20]. Decane hydroconversion, meanwhile, allows for evaluating the type, strength and distribution of the acid sites in the solids [21].

Although, as already mentioned, pillarized vermiculites have shown their great potential in hydroconversion reactions, it is striking that there are still no reports of delaminated vermiculites for this type of reactions, which could favor the traffic of bulky molecules

for adsorption and catalysis processes as well as providing a greater availability of acidity than that offered in the pillared mineral.

In this context, this work has focused on the study of the evaluation of the main physicochemical properties generated by the delamination and subsequent incorporation of AlZr and AlCe species in a raw vermiculite. With special emphasis on the evolution of acidic properties, to our knowledge, there are still no reports in the literature regarding delaminated vermiculite using HTT for the reduction of the layer charge, an acid treatment to achieve the exfoliation of the mineral sheets, nor of its modified acid potential with AlZr or AlCe species, nor of the characterization of acidity using CO-FTIR and dehydration dehydrogenation of propanol. This contribution allows for generating tools for the use of these materials in future applications.

Experimental

Starting material

The starting mineral used was a vermiculite from the Santa Marta region, Colombia, which has been the subject of other studies and part of its characteristics have been previously reported [8, 22]. Its cation exchange capacity is 1.1 meg·g^{-1} and has the following structural formula:

$[(Si_{3.04}Al_{0.92}Ti_{0.04})(Al_{0.11}Fe^{3+}_{0.35}Fe^{2+}_{0.07}Mg_{2.41}Mn_{0.003})\ O_{10}(OH)_2]Ca_{0.21}K_{0.05}Na_{0.10.}$

Modification of the mineral. Delamination process.

The vermiculite was subjected to a HydroThermal Treatment (HTT) previously reported [8, 22], which allows for the reduction of the mineral layer charge by eliminating part of the aluminum located in the tetrahedral sheet, thus producing a layer charge reduction facilitating the following modifications. Subsequently, a 10% dispersion of the vermiculite in distilled water was left in contact with a solution of 2 M nitric acid (10 mL HNO_3·g^{-1} vermiculite), for 4 h in constant agitation and between 90-95 ºC to generate the

opening and/or exfoliation of the mineral sheets. The solid obtained was washed with distilled water by centrifugation, dried at 60 °C, and calcined at 400 °C for 4 h, increasing the temperature at a rate of 10 °C·min^{-1} [8, 22].

Synthesis and incorporation of the AlZr or AlCe phase.

The incorporation of the AlZr and AlCe phases in the delaminated supports was carried out using $Al(NO_3)_3$, $ZrOCl_2$ and $Ce(NO)_3$ [6] as precursor compounds. A 90:10 ratio of aluminum-metal [6, 23] was handled in a 0.1 molar solution which was subsequently hydrolyzed with NaOH, maintaining an OH/metal ratio=2 [24]; this solution was stirred for 1 h at 300 rpm and subsequently brought to pH=9 using 1 M ammonium hydroxide and generated the formation of a solid which was washed to a conductivity close to that of deionized water [25].

This solid was dissolved in acid with an H^+/metal ratio = 0.27 and taken to ultrasound for 10 min. Subsequently, impregnation was carried out on the clay at 30%, and it was stirred for 2 h, followed by drying overnight at 60 ℃. Finally, the solids were calcined at 400 °C for 4 h with a temperature ramp of 10 °C·min^{-1} [25]. The solids obtained were denominated VN for the raw vermiculite, VD for the process of delamination, and VD-AlZr, VD-AlCe, for the delaminated minerals subsequently modified with AlZr and AlCe respectively.

Characterization

The X-ray diffraction patterns were performed on a PANalytical X'PertPRO MPD equipment with Cu copper anode (λ = 1.54056 Å), using a speed of 0.02θ with 2s. Prior to analysis, solids were screened in a 100 ASTM mesh, diffractograms were obtained at room temperature [25–27].

The XPS measurements were performed on a X(NAP-XPS) *Specs* with a PHOIBOS 150 1D-DLD analyzer, equipped with a monochromatic source Al-Kα (1486.7 eV, 13 kV, 100

W) with a step energy of 30 eV and step of 0.1 eV. 30 measurement cycles were performed and charge compensation of 2 2 eV and 20 µA was used.

The specific surface area was obtained from the nitrogen adsorption isotherm at -196 °C with a Micromeritics ASAP 2020 instrument. For the determination of the specific surface area the BET model was used, the external and micropore area was calculated using the Harkins-Jura equation and the pore size distribution with the BJH model, based on the Kelvin equation and applied in the desorption branch of the isotherms [25, 27, 28]. Total acidity analyzes (NH_3-TPD) were carried out with a Micromeritics AutoChem 2920 device. 200 mg of the solid were used, which were degassed in He for 30 min at 350 °C, with a temperature ramp of 10 °C·min^{-1} and a flow of 30 mL·min^{-1}. Subsequently, it cooled to 50 °C and ammonia was adsorbed for 30 min (5% NH_3/He). The assembly was then purged with He for 1 h and finally brought to 700 °C with a ramp of 10 °C·min^{-1} [25, 29].

Diffuse reflectance infrared Fourier-transform spectra (DRIFTS) were measured on an FT-IR spectrometer (IR Tracer-100) equipped with a Harrick Praying Mantis accessory and a high-temperature reaction chamber for diffuse reflectance infrared Fourier transform spectroscopy (DRIFTS) studies of catalysts, which is carried out according to previous reports [25, 27, 30, 31]: i) Pre-treatment of the solid at 400 °C with an N_2 flow of 30 mL·min^{-1} for 1 h, ii) Adsorption NH_3 (g) for 15 min at room temperature at 30 mL·min^{-1}, iii) Desorption for 30 min with a N_2 flow at 30 mL·min^{-1} at room temperature experiments in a Praying Mantis chamber. All spectra were averaged from 150 scans collected at a resolution of 4 cm^{-1} and were converted to an absorption spectrum using the Kubelka–Munk function.

For the adsorption of CO at low temperature analyzed by FTIR, the solids were pressed on self-supporting wafers of approx. 12 mg cm^{-2} and activated in a quartz cell placed in

the IR beam, at 550 °C in a vacuum for 1 h. After pretreatment, the solids were exposed to CO doses until saturation at -196 ºC by using a trap cooled by liquid nitrogen and then evacuated. The transmittance spectra were recorded with a THERMO NICOLET Avatar 380 FTIR Spectrophotometer, equipped with a DTGS/KBr detector and accumulating 128 scans at a spectral resolution of 4 cm^{-1}. The spectra were processed using Nicolet OMNICTM software [32].

For the dehydration-dehydrogenation analysis of 2-propanol, a pretreatment was carried out at 50 $mL \cdot min^{-1}$ of He for 1 h at 400 °C, then 50 $mL \cdot min^{-1}$ of He was passed through a saturator of 2-propanol at 0 °C. The saturated mixture was fed into a fixed bed reactor loaded with 100 mg of solid increasing the temperature from 100 to 400 °C at 10 $°C \cdot min^{-1}$. The reaction was followed by mass spectrometry, using a Balzers Thermostar controlled by Balzer Quadstar 422 software with capabilities for quantitative analysis. Signals from 1 to 200 m/z were recorded. Among them, 45, 43, 41, 18 and 2 m/z were assigned to 2-propanol and the main reaction products: acetone, propene, water and hydrogen, respectively [33].

Decane hydroconversion was performed using 300 mg of the solid (particle size between 125 and 150 μm) in a U reactor (with internal diameter of 3 mm, length of 26 cm, with a bulb of 5 cm with internal diameter of 1 cm, the bubble was to the first 4 cm of the reactor. The reactor is filled with SiC and the catalyst is located inside the bulb) at atmospheric pressure. The pretreatment of the solid was carried out at 400 °C at a heating rate of 10 $°C \cdot min^{-1}$ and was maintained in a flow for 2 h 50 $mL \cdot min^{-1}$ of dry air. Then, a cleaning with N_2 for 15 min and a flow of H_2 was passed for 2 h in order to activate the catalyst. The catalytic activity was carried out with a H_2/hydrocarbon ratio of 17, with a total flow of 16 $mL \cdot min^{-1}$ and the WHSV = 1.16 h^{-1}, in a temperature range of 150 °C to 400 °C, making measurements at 25 °C intervals. The reaction products were analyzed online by

gas chromatography using a Shimadzu GC-17 chromatograph, with a ZB-1 column (60m x 0.53mm x 0.32 μm) and a FID detector. The catalytic activity was expressed in terms of conversion, yield to isomerization (monobranched: methylnonanes, dibranched: ethyloctanes, and tribranched: propylheptanes) and cracking (all products with less than 10 carbon atoms), as previously reported, the error is ±3% in all cases [25, 27, 31, 34].

Results and discussion

Structure and Texture

Fig. 1. registers the characterization by XRD of i), the raw mineral, ii) following the HTT, (iii) following the delamination process and iv) with the incorporation of AlZr and AlCe. As can be seen, the reflection clearly defined for VN at 6.40 °2θ, indicates that the starting vermiculite is of high purity and with a high degree of crystallinity [22]. This can be attributed to the highly localized negative charge exhibiting a high three-dimensional order [22]. In addition, the characteristic reflections for vermiculite (9.8, 12.38, and 18.60, °2θ) are observed according to the JCPDS records: 01-076-0847 and 00-016-0613 [11, 35].

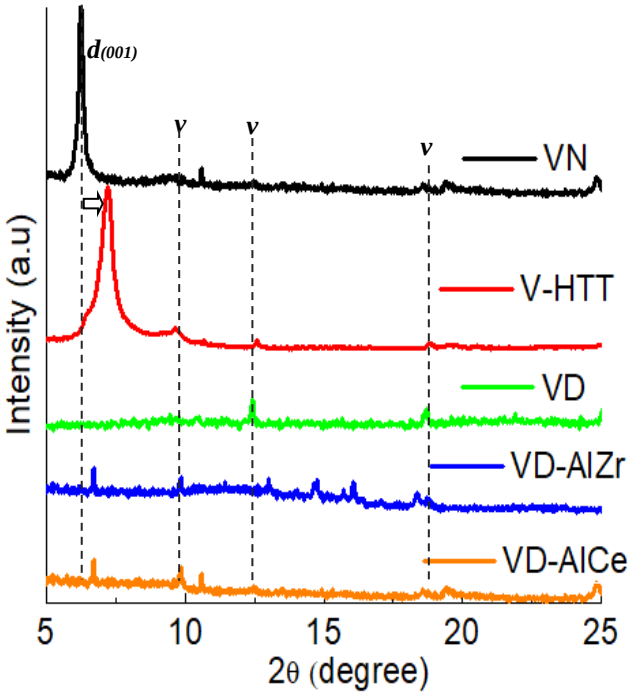

Figure 1 Diffractograms of raw vermiculite (VN), following hydrothermal treatment (V-HTT), delaminated (VD) and the different modified solids. *v = vermiculite.*

The reflection found at 6.40 °2θ corresponds to an interlayer space of 14.9 Å. After the HTT process, a shift towards higher º2θ values is observed, which indicates a decrease of interlayer space between 12 and 13 Å, this effect is attributed to a closing of the sheets due to the extraction of Al from the tetrahedra of the clay showing that only the HTT process does not have the capacity to delaminate the material.

After the acid treatment, the disappearance of said reflection (6.40 °2θ) is observed, which indicates an effective delamination of the vermiculite, indicating the obtaining of a face-face, face-edge and edge-edge order in the mineral [36], evidencing in this case the beneficial effect of this process on the structural properties of the mineral.

Finally, the absence of crystalline phases for Zr (17.43, 28.2, 31.45, 34.25, °2θ) or Ce (28.54, 33.11, °2θ) oxides for the materials is observed, which can be attributed to the fact that Zr or Ce are highly disordered on the surface [37] or, also, to the low percentage of these oxides used with a high dispersion located below the detection limit of the technique [38].

In contrast, the results by XPS (Fig. 2.) suggest the existence of interaction between Zr or Ce cations with the mineral. In the case of Zr, the 3d signal registers a doublet located at 182.8 eV with a separation of 2.4 eV (Fig. 2a.), corresponding to the species Zr^{4+} in whose first coordination sphere oxygen is found [39]. These values indicate the absence of ZrO_2, which presents a signal at 182.2 eV (corroborating what is described by XRD). The shift in signals with respect to pure ZrO_2 suggests the formation of Zr^{4+} species linked to more electronegative species [39]. Therefore, is likely that the Zr is interacting with the mineral structure formed by the species: i) $AlZrO_X^-$, ii) ZrSiO-(H), iii) OH groups associated with Zr, as reported for pillared clays or iv) Zr-Si whose presence is evidenced by the shift of Si 2p in the XPS verifying that the Zr favors both the existence of species

Si-O(H)-Al, ZrSiO-(H) and Zr-O-H [40] leading to an increase in the acidic characteristics of the materials.

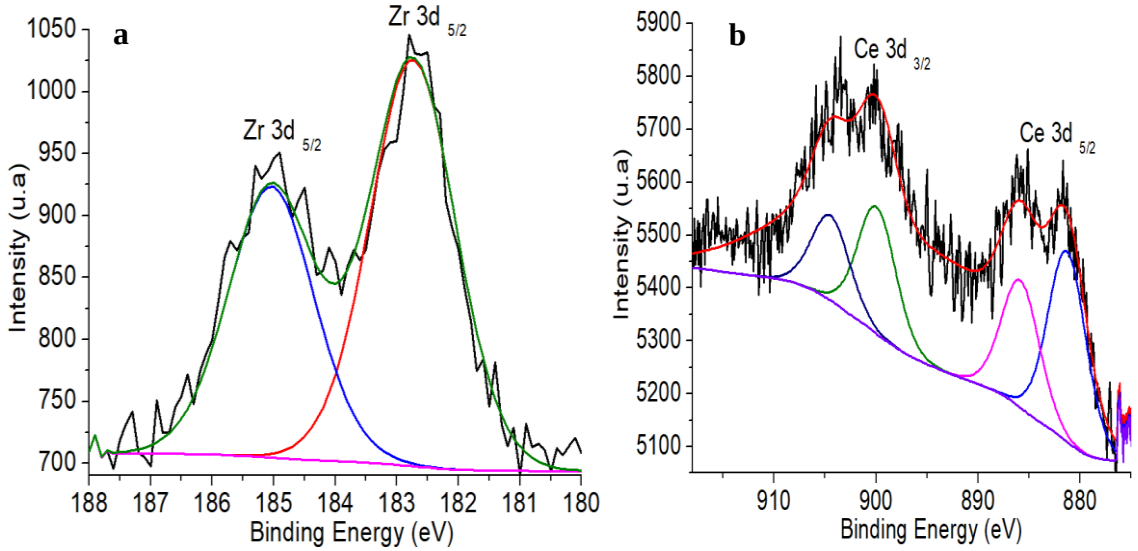

Figure 2 XPS spectra of core level 3d of VD-AlZr (a) and VD-AlCe (b).

On the other hand, the XPS spectra corresponding to the 3d level of Ce and associated with Ce^{3+} (Fig. 2b.), record a signal at 881.9 eV assigned to the $3d_{5/2}$ broadcast with its corresponding satellite at 886.3 eV, while the signal at 900.4 eV is assigned to the $3d_{3/2}$ broadcast with its respective satellite at 904.9 eV [41]. And the latter is also from Ce^{3+}. The absence of the signal at 916 eV indicates that the tetravalent state of Ce is not present [42]. Indicating that possibly all the Ce in the structure is formed Ce-Al- or Ce-Si-O species [43] which would explain the increase in acidic properties when this cation is used. These results found by XPS are like those reported in other materials, as well as in pillared clay minerals [39, 44].

On the other hand, Fig. 3(a). illustrates the nitrogen adsorption isotherms for the raw mineral, following the HTT process, delamination and with the incorporation of AlZr and AlCe. Table 1 records the respective textural parameters. The unusually small specific surface area of raw vermiculite (3 $m^2 \cdot g^{-1}$, this value agrees with previously reported results and with that reported for vermiculites from other provinces [5, 11, 14]) is caused by the high interlayer charge of the clay that generates a lower access to interlayer space

and consequently a smaller specific surface area. This same area is maintained after the HTT process, evidencing that this process does not generate an opening of the sheets but, on the contrary, it contracts them, evidencing that there are no great structural and textural differences between the raw mineral and after the HTT, as was evidenced by the XRD.

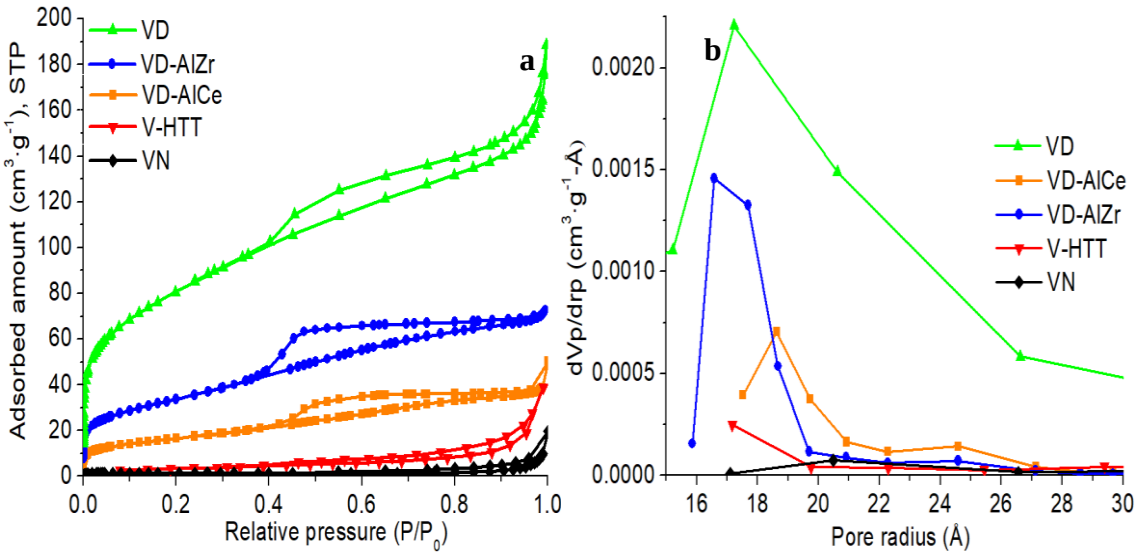

Figure 3. Adsorption isotherms (a) and pore size distribution (b).

However, the effect of the delamination process drastically increases the specific surface area of the raw mineral, obtaining a vermiculite (VD) with more than 273 $m^2 \cdot g^{-1}$ (almost 90 times more area than the original) which is a value close to or higher than the literature reports for vermiculites with similar treatments [35]. The disappearance of the 001 reflection (basal reflection) and the increase in specific surface area, demonstrates the successful delamination of the mineral. This is a first step to generate access to the intrinsic acid sites of the mineral and, at the same time, to facilitate roads for molecular traffic. The solids obtained after the delamination process exhibit a type IV isotherm with a H4 hysteresis typical of lamellar solids.

As is recorded in Table 1, the delamination process essentially generates mesoporosity which represents, in all the solids, between 90 and 98% compared to 2 and 10% of microporosity. This noticeable difference is a consequence of the opening of the sheets to an edge-face position [45]. However, the incorporation of the AlZr and AlCe species

generates a decrease in the specific surface area of the delaminated clay, which is attributed to the fact that these species can cover the external surface of the mineral [46]. The incorporation of the AlCe species into the VD support generates a decrease in the BET area (78%) close to double of that which occurs with the incorporation of AlZr (43%). This behavior may be due to the fact that the polyhydroxocation of AlCe, formed by the addition of small amounts of Ce^{3+} to a solution of Al^{3+}, probably consists of four units of the Al_{13}^{7+} polymer joined by a tetrahedrally coordinated Ce atom, making it more bulky in comparison with the AlZr cations which only have one unit of Al_{13}^{7+} [47]. Other works related to the hydrolysis of AlCe mixed solutions suggest the formation of polyhydroxycationic species with a strong AlCe interaction and the presence of polynuclear species of a chemical nature different from that of the simple Keggin ion [47], which generates a greater blockage on the support, compared with the AlZr species.

Table 1 Physicochemical characterizations for natural mineral and modified solids.

Solid	Specific surface area ($m^2 \cdot g^{-1}$)[a]				Pore volume [c] ($cm^3 \cdot g^{-1}$)		Pore radius (Å)[e]	Total acidity		$T^oC_{(maximum)}$ NH_3-TPD[h]	B/L[i]
	BET	Micro	Meso	$S_{(External)}$ [b]	Micro [b]	Total [d]		µmol·g^{-1}[f]	U.A[i]		
VN	3	3	--	---	---	---	20.0	3	4	97	1.0
V-THT	6	4	2	---	0.0001	---	17.0	---	---	---	---
VD	274	17	257	270	0.0062	0.29	17.0	257	566	121	1.4
V-AlZr	119	4	115	116	0.0014	0.11	16.5	371	810	137	0.9
V-AlCe	59	3	56	56	0.0011	0.077	18.5	392	851	127	1.1

[a]: Sensitivity of the technique +/- 10 $m^2 \cdot g^{-1}$
[b]: The value of t was calculated using the Harkins-Jura equation.
[c]: Liquid volume
[d]: Determined using the Gurvitsch method
[e]: margin of error +/- 0.5
[f]: µmol of $NH_3 \cdot g^{-1}$: total acidity determined, Sensitivity of the technique +/- 3 µmol of $NH_3 \cdot g^{-1}$
[g]: U.A: Areas determined by Brönsted and Lewis acidity at 25 ºC
[h]: Error range +/- 1 ºC
[i]: B/L: relationship between Brönsted acidity and Lewis at 25 ºC

Fig. 3(b). illustrates the pore size distribution of the different materials. The existence of high pore volumes in the mesoporous region is observed in the radius between 15 and 50 Å, which is typical of delaminated clays where the formation of mesoporosity is favored [45]. In addition, these values are very close to those reported in the literature for vermiculite delaminated by acid treatment [5].

Both the raw mineral and the HTT material have an almost null population of pore diameter between 15 and 50 Å. However, following the delamination process this pore diameter population grows 20 times compared to VN, which agrees with the increase in specific surface area. In addition, this distribution indicates that the mesoporous system is more heterogeneous for delaminated mineral because small pore contributions with different sizes are evident. After the incorporation of AlZr and AlCe, the solids obtained have a more homogenous pore size distribution compared to the delaminating material, observing the clear effect of said species on the average size and pore distribution. In addition, it is observed that Ce causes a shift towards a larger pore radius (VD-AlCe = 18.5 Å), compared to Zr (VD-AlZr = 16.5 Å), which suggests that the use of Ce generates less pores, but with a larger size (mesoporosity), compared to Zr. The increase in the pore radius can be an advantage in processes where the porous structure is blocked with coke, since the obstruction of the material could be less severe than in structures with a lower average pore radius [45].

Characterization of acidic properties.

Considering that in general terms there is no technique that provides all the information of interest in relation to the acid properties of the solids (number, type and strength), the characterization of these properties was carried out using NH_3-TPD and NH_3-DRIFTS, adsorption of CO at low temperature and, in parallel with the catalytic behavior, the dehydration-dehydrogenation of 2-propanol and the hydroconversion of C_{10} was carried out.

Table 1 records the results obtained in the determination of the acidity by NH_3-TPD for the different solids. The total acid content of VN (3 μmol of $NH_3 \cdot g^{-1}$) corresponds, evidently, to the intrinsic acidity of this clay mineral, in which the desorption signals of NH_3 are absent or very weak following the treatment with ammonia [48]. This effect is

associated with the difficult access of the probe molecule to the acid sites of the material, preferably located in the reduced interlayer space with a high charge density. The VN after the HTT does not present differences with the raw material.

The magnitude of the impact generated by the delamination process on the textural properties already discussed is consistent with the effect caused by said process on the acidity of the solid. In effect, delamination generates an increase in acidity close to 90 times in VN (going from 3 to 257 μmol of $NH_3 \cdot g^{-1}$), coinciding with the same order of magnitude of the increase observed with the BET area and higher than that reported for modified vermiculites [49]. In this way, if the effect of the process of delaminating vermiculite is compared with the same process in another mineral such as bentonite, it is noted that in the first case delamination causes an increase in acidity close to 90 times in VN (passing from 3 at 257 μmol of $NH_3 \cdot g^{-1}$), while in bentonite it is doubled (from 56 to 110 μmol of $NH_3 \cdot g^{-1}$) [25], coinciding with the same order of magnitude of the increase observed with the BET area. The reason for this behavior is the same as already discussed and is related to the opening of the sheets and the consequent increase in the exposure of areas and acidic sites, corroborating the positive effect of delamination as the first process to potentiate the intrinsic acidity of vermiculite.

In addition, it should be noted that the acidity of delaminated vermiculite is more than double that achieved with the delaminated bentonite [25], which is a consequence of the difference in interlaminar charge density between vermiculite and bentonite, being noticeably higher in the VN due to the greater number of isomorphic substitutions of Si^{4+} for Al^{3+} in the tetrahedral layers compared to those present in bentonite. The decompensation of charge generated by the described isomorphic substitution, promotes the formation of sites with an acidic character either because the deprotection of positive

charges allows for the acceptance of electronic pairs (Lewis acidity) or because they can capture protons and then yield them (Brönsted acidity) [6].

With the insertion of the AlZr or AlCe species as an additional step to extrinsically increase the global acidity potential of the mineral, it can be observed (Table 1) that in both cases an increase in acidity is generated attributed to the generation of new acid centers, without being able to discriminate between Lewis or Brönsted sites. However, it is observed that the VD-AlCe solid presents a greater amount of ammonia adsorbed (close to 10%) compared to VD-AlZr, which would be in direct relation with the protons of each solid (each mmol of NH_3 corresponds to 1 mmol proton), this increase in the number of acid sites has been reported for acid catalysts with Ce [50], however, the use of Ce^{3+}, Ce^{4+} ions and their influence on acidic properties generates controversy and knowledge thereof is still limited [50]. For the catalysts with Zr, said increase in acidic sites is associated with the production of protons caused by the dehydration of the polyhydroxication introduced in the interlayer space [51] or as a consequence of the protonation of the Si-O (H) -Al bond induced by a pH decrease characteristic of Zr solutions [52].

In this way, a comparison of VD-AlZr with a bentonite with the same treatment [25] shows a notable increase in the material obtained from vermiculite. In addition, the two delaminated minerals generate a notable increase in acidity compared to that reported in the same minerals but modified through the pillarization process [8, 31]. This difference is attributed to the fact that delamination allows for greater access to the intrinsic acid sites of the natural mineral and, in addition, generates a larger BET area and particularly a larger mesoporous area compared to pillarized minerals (BP-AlZr; BET = 109, Smeso = 30, VP-AlZr; BET = 118, Smeso = 48) [6, 31], which permits accepting a greater quantity of AlZr species with a better surface distribution.

For the AlCe system, a trend similar to that discussed for AlZr is observed, obtaining greater BET areas and especially mesopores, compared to pillarized minerals (BP-AlCe; BET = 55, Smeso = 25, VP-AlCe; BET = 30 , Smeso = 12) [6, 23], favoring the greater distribution of AlCe species on the surface (consistent with the XPS results), improving acidic properties, even greater than the delaminated bentonite and the incorporation of the same species [25].

In the case of the maximum ammonia desorption temperatures, following the delamination process an increase in the number of acid sites with greater strength for VD is observed, going from VN=3 μmol of $NH_3 \cdot g^{-1}$ (97 ºC) to VD = 257 μmol of $NH_3 \cdot g^{-1}$ (121 ° C). On the other hand, the incorporation of the AlZr and AlCe species slightly increases the desorption temperatures by 16 and 6 ºC respectively, attributed to the fact that the use of Zr for the modification of clays increases the acid strength [53], which is mainly associated with Lewis type acidity [54]. In the case of Ce, this increase is related to the stabilization of Brönsted type acid centers [55]. These results corroborate that the incorporation of these species in this delaminated mineral not only increases the number of sites (from 257 to 392 μmol) but also the strength of these (from 121 to 137 ºC) as has been reported [56].

To have a better understanding of the type and strength of the acid sites obtained, the use of NH_3-DRIFTS and the adsorption of CO at -196 ºC were used as complementary techniques to discriminate between the Brönsted or Lewis types and to understand the role of the M^{+3}, M^{+4} cations present in the solids.

Fig. 4. illustrates the infrared spectra (in black) corresponding to the different materials obtained after degassing the samples at 400 ºC in a N_2 atmosphere for 1 h. In all cases, the signals characteristic of the presence of OH groups are observed in the wave number range of 3400 to 3650 cm^{-1}, characteristic of clay minerals. On the other hand, the signals

can also be observed at 3600 cm^{-1} and 3650 cm^{-1} which are attributed to SiOH groups close to aluminum in tetrahedral coordination and to AlOH [57, 58] species, respectively. The bands around 3620-3630 cm^{-1} correspond to the characteristic vibrations of the structural OH groups; The shoulder around 3270 cm^{-1} can be attributed to a water overtone linked with a vibration visible around 1650 cm^{-1}. The band at 1200 cm^{-1} is due to the vibration of the silicon-oxygen bond, within which are included the vibrations of the apical silicon-oxygen units which are perpendicular to the sheets (oxygen atoms shared by tetrahedral and octahedral sheets) and the stretching vibrations of this bond within the tetrahedral sheet. A broad band around 1200 cm^{-1} corresponds to quartz O-Si-O [59].

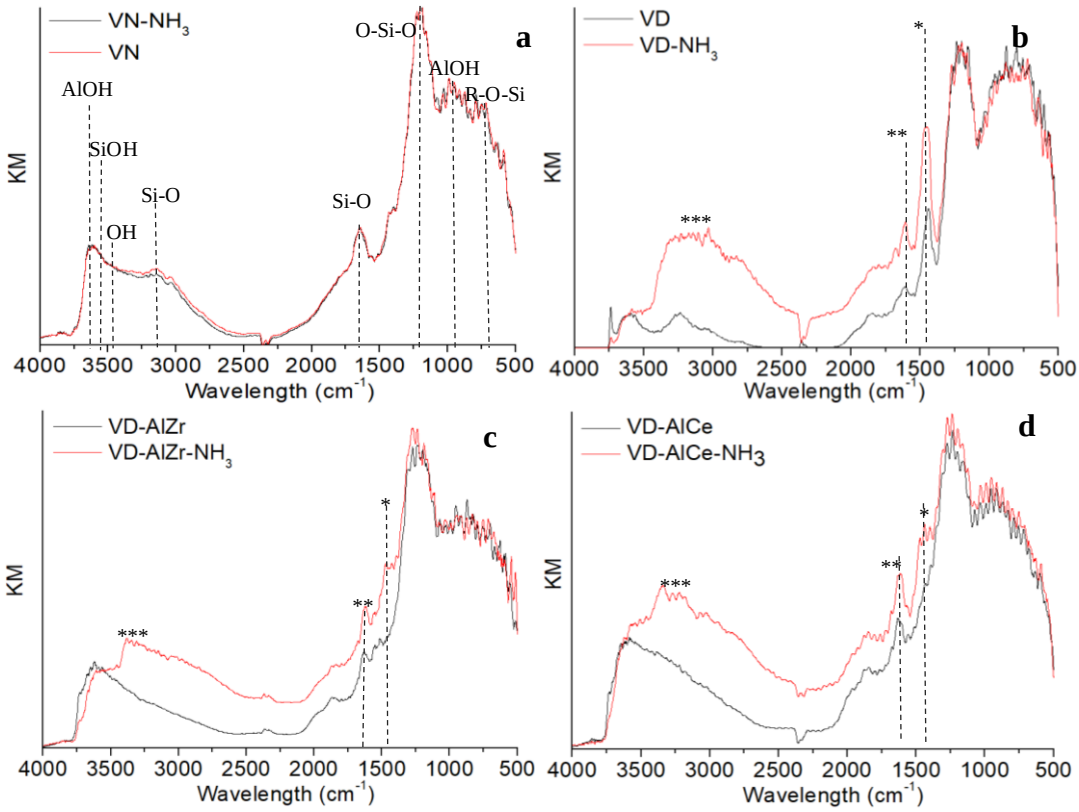

Figure 4. DRIFTS spectra at room temperature, then 1 h at 400 °C in N_2 of a) VN, b) VD, c) VD-AlZr, and d) VD-AlCe, before (black) and after (red) NH_3 adsorption. * Brönsted acid sites, ** Lewis acid sites and *** physiosorbed ammonia.

The band at 610 cm^{-1} is related to the perpendicular vibration of the octahedral cations (R-O-Si), where R can be Mg or Al [60]. The partial substitution of magnesium by Al and Fe is reflected in the variety of complementary signals in this same region. The groups

AlOH, AlFeOH and AlMgOH are related to vibrations at 925, 880 and 750 cm^{-1} respectively [60].

On the other hand, the main differences of the spectra between the different solids are found in the hydroxyl region located between 3000 and 3600 cm^{-1} (Fig. 5.). There, raw vermiculite has a broad band and poorly defined signals, which can be attributed to a greater amount of water associated with its structure [61] compared to the mineral after the delamination process which presents a clear signal at 3750 cm^{-1}; these signals are assigned to bridged hydroxyl groups through pairs Al^{VI}-Al^{VI} and Al^{IV}-Al^{VI} of the delaminated minerals [62]. The spectra for the VD-AlZr and VD-AlCe solids are like that of the non-delaminated material. However, there is an increase in the width and relative intensity of the band close to 3680 cm^{-1} that can be associated with "external" silanol groups which, following the process of incorporation of Al-M species, are more exposed on the surface. On the other hand, when the surface charge is concentrated in the oxygens involved in the Si-O-Si bonds, the hydrogen bound to the hydroxyl groups of these oxygens absorbs in the region near 3440 cm^{-1}, overlapping the region of absorption associated with water-water connections and increasing the amplitude of the band [63, 64]. In addition, a change in the region of 3000 to 3800 cm^{-1} is observed for the solids VD-AlZr and VD-AlCe with respect to the delaminated material, with a wide shoulder in the region of 3620-3300 cm^{-1}, suggesting a possible change in the structure of the clay during the process of incorporation of the metals originated by the presence of small strongly polarized groups such as Al^{3+}, due to the Zr or Ce located in the clay sheet [64]. The small signals observed at 3746, 3735 and 3675 cm^{-1} for the materials after the incorporation of AlZr or AlCe are characteristic of hydroxyl groups coordinated to two or three M^{4+} cations. On the other hand, the bandwidth at 3550 cm^{-1} can be attributed to the presence of the amorphous phase of zirconia or ceria [65] which correlates with the

XRD results obtained, where it was concluded that the incorporated species are highly disordered. This characteristic is highlighted in the spectrum region around 3000 cm^{-1}, where the bands attributed to the stretches of OH groups, both free and structural [60], are greater in the materials with Ce than in those with Zr.

In addition to the identification of the typical functional groups of a clay, the evaluation of the acidic properties of the solids was carried out using DRIFT and the NH_3 as a probe molecule. In this way, the interaction between the acid support and the probe molecule was studied, which generates mainly two vibration groups: i) at 1425-1460 cm^{-1} corresponding to the presence of protonated ammonia associated with the interaction with Brönsted sites and ii) 1600-1640 cm^{-1} of ammonia coordinated to Lewis acid sites [31, 34].

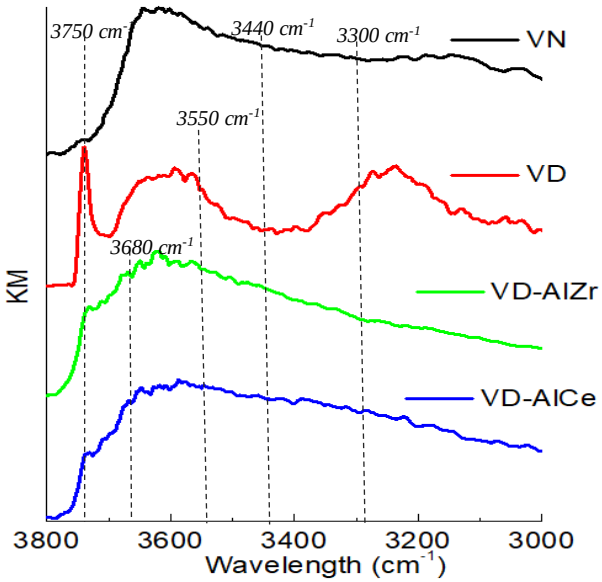

Figure 5 DRIFTS spectra in the OH region, of the different solids, after degassing at 400 °C for 1 h in N_2.

As illustrated in Fig. 4(a), the VN before and after the adsorption of ammonia does not present significant differences, despite the potentially acidic sites generated by the high interlayer charge density that characterizes this material [48], which is consistent with the results found by NH_3-TPD. This apparent contradiction is explained by the structural position of the acid sites in the mineral that hinder access and interaction with the probe

molecule. After the delamination process an increase in the acid sites was observed, reflected in the growth of the bands at 1625 and 1450 cm^{-1} after the adsorption of ammonia (Fig. 4(b)), confirming the presence of the acid sites belonging to the material and now available, in coherence with the delamination process as a first step to potentiate the raw acidity of the mineral. On the other hand, it was corroborated that the incursion of the AlZr and AlCe species also generates an increase in acidity, as recorded in Fig. 4(c-d), confirming that the use of these cations allows for the controlled modulation of the acidic properties of the materials, improving the extrinsic acidity of the same.

To semi-quantify the increase in the acid properties of the starting minerals and following each of the modifications, the proportion and strength of the acid sites during desorption of NH_3 from ambient temperature to 400 ºC was determined. For this, the bands corresponding to the Brönsted and Lewis sites were integrated in the spectra at different temperatures, assuming that the concentration is proportional to the area under the curve [31]. Fig. 6. records, by way of illustration, the spectra obtained for VD after degassing and the interaction with NH_3 at different temperatures, evidencing the decrease of NH_3 adsorbed in the modified mineral as a function of the temperature.

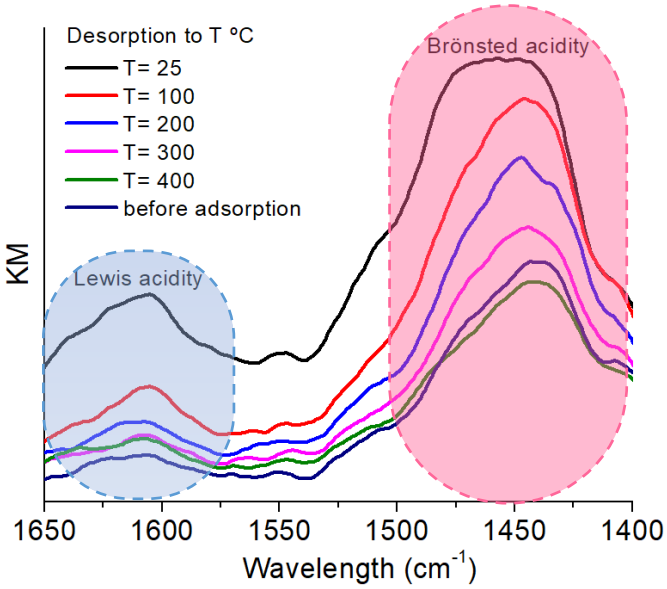

Figure 6. DRIFTS spectra of delaminated vermiculite, after degassing, and desorption of NH_3 at each of the different temperatures.

In this way, the type, number and strength of the acid sites for the raw mineral, delaminated and following the incorporation of the AlZr and AlCe species were determined. Fig. 7. describes the trends found in the NH_3 desorption as a function of the temperature between 25 ºC and 400 ºC. These results corroborate the difficulty of accessing the VN acid sites and the effect of the delamination process in exposing the intrinsic acid sites of the mineral, which present a great strength, if compared to a bentonite under the same treatment [25], as indicated by the slopes of the desorption curve.

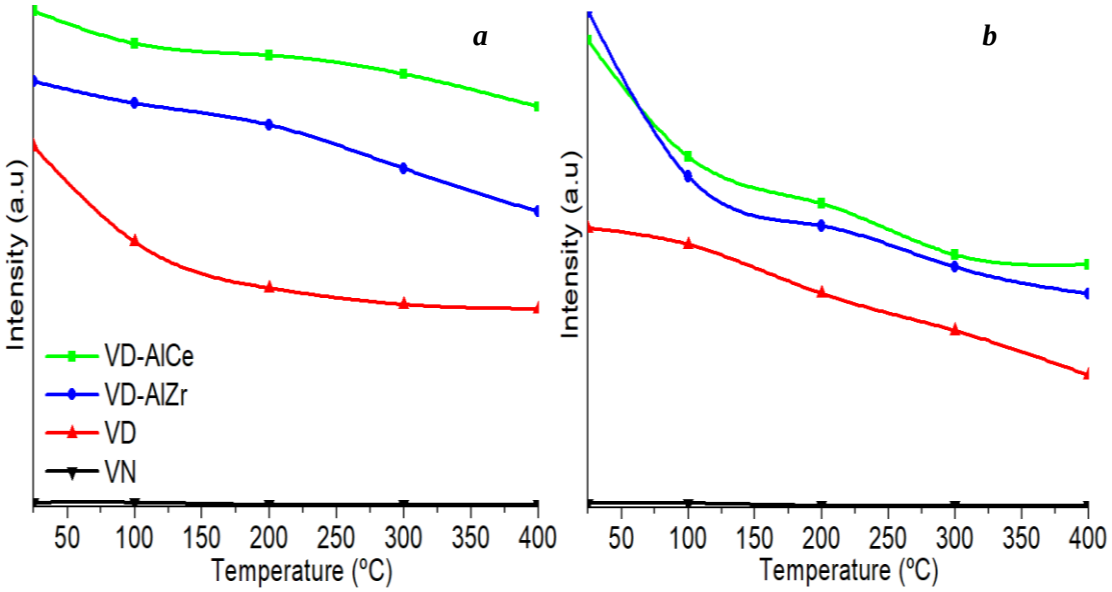

Figure 7. Area under the curve of the bands at 1450 cm^{-1} Brönsted acidity, (a) and 1650 cm^{-1} Lewis acidity (b), as a function of the degassing temperature after adsorption with ammonia.

On the other hand, the beneficial effect on the acidic properties generated by the incursion of AlZr and AlCe metals is clearly observed, which is mainly associated with the acidic character of the metal oxides incorporated on the surface of delaminated minerals and discussed previously. It was also determined that it is the solids with presence of Ce that present the highest acid values determined by both NH_3-TPD and NH_3-DRIFTS as shown in Fig. 8.

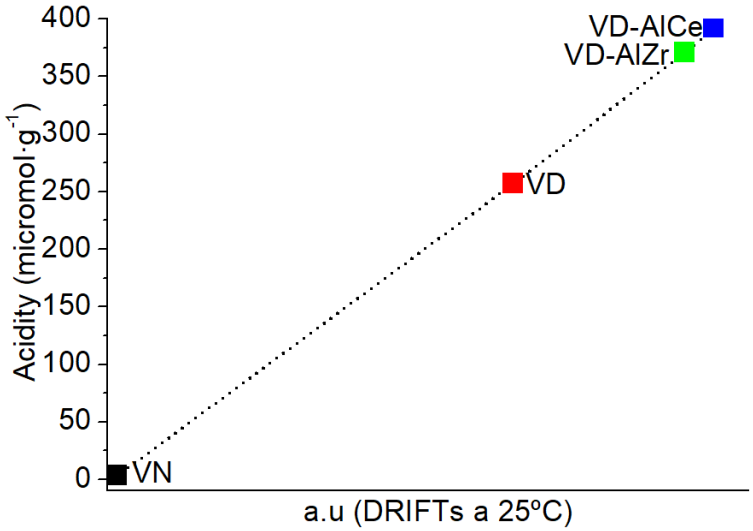

Figure 8. Correlation between total acidity determined by NH_3-TPD and NH_3-DRFITS at 25ºC.

In general, the solids with Ce exhibit mainly Brönsted acidity, which is attributed to Ce's ability to stabilize said acid centers [55]. In this sense, the ratio of Brönsted acid sites to Lewis acid sites (B/L) is higher for AlCe modified solids compared to those modified with AlZr (Table 1), highlighting a greater formation of Lewis acid sites when the AlZr species are incorporated, consistent with literature reports [66]. It is important to note that for solids modified with AlZr and AlCe both types of acidity (Brönsted and Lewis) are still maintained at high temperatures (400 ºC), indicating their stability. Finally, it is highlighted that the solids with Ce in their structure have a higher acid strength, exhibiting a greater number of protonic acid sites.

To obtain information regarding the resistance and number of Lewis acid sites and to relate this to the observed differences in the behavior of the acidic properties the CO adsorption was carried out at low temperature (-196 ºC) followed by FTIR measurements. The IR spectra of the solids were recorded after 1 h of activation at 550 ºC in a vacuum, in the stretching regions for increasing amounts of adsorbed CO (with the spectrum of the activated sample subtracted as a reference) for the different materials (Fig. 9). This adsorption of CO generates coordination bonds with sites of acidic Lewis cations, causing a disturbance of the hydroxyl group vibration on the surface that results in an upward displacement of the CO stretch mode at 2143 cm^{-1} compared to the one registered for the

solid without adsorption. The extent of these changes provides useful information concerning the Lewis strength of acid sites in solids [67].

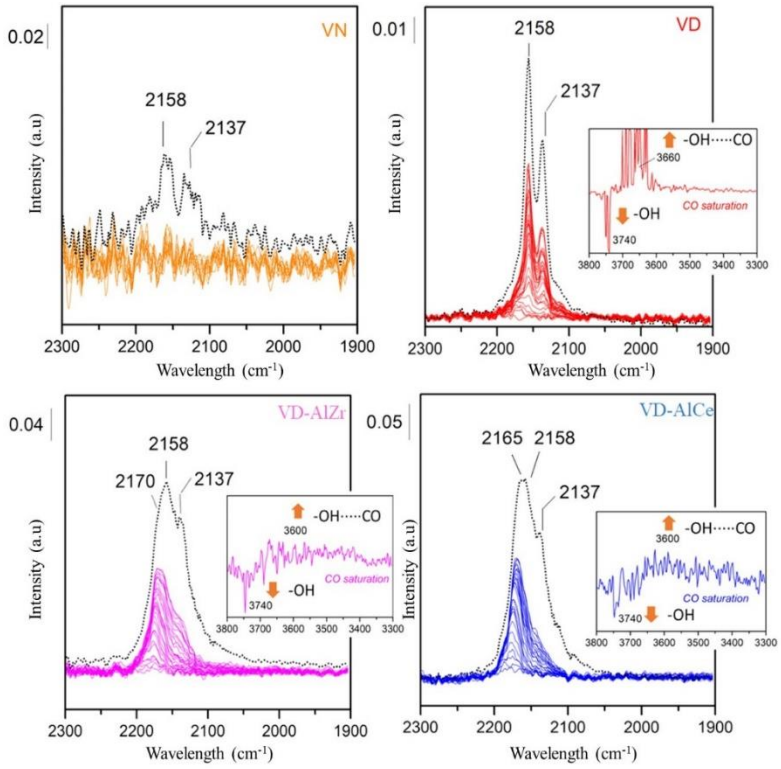

Figure 9. FTIR difference spectra after the adsorption of CO in the ν region (CO) for the different solids.

It is observed that the CO adsorption results in the appearance of a single band in the ν region (CO) at between 2140 and 2170 cm^{-1}, and the increase in CO pressure leads to an increase in its intensity. In this sense, the number and strength of the acid Lewis sites are compared to the different solids (Fig. 10). It's observed that the raw mineral does not have adsorption of CO, which is attributed to the few acid sites to which this material has access to. Moreover, after the delamination process, an increase in the adsorption of CO is observed, associated with the Lewis acid sites to which it now has access, this effect agrees with what is observed by the NH_3-TPD and NH_3-DRIFTS of ammonia. On the other hand, after the incorporation of AlZr and AlCe, there was a pronounced increase in the number of Lewis acidic sites in the materials, being more significant for AlCe in comparison with AlZr (Fig. 10 (a)). In this way, to give a practical interpretation of CO

adsorbed in cations of Lewis sites, a correlation has been proposed between the CO interaction energy and the wavenumber change illustrated in equation 1 [68].

$$\Delta H\left(\frac{kJ}{mol}\right) = 10{,}5 + 0{,}5\,\Delta\nu\,(CO) \qquad equation\ 1$$

For the case of raw and delaminated mineral, signals were found at 2135 and 2158 cm^{-1}. The band at 2135 cm^{-1} appears very close to the CO gas and can be attributed to the weakly adhering CO in the pores of the clay [68], in addition, the band at 2158 cm^{-1} could be associated with the interaction of the silanol or aluminol groups with the CO [68], generating corresponding energies to an ΔH of -8 and 13 $kJmol^{-1}$ respectively, (Fig. 10(b)).

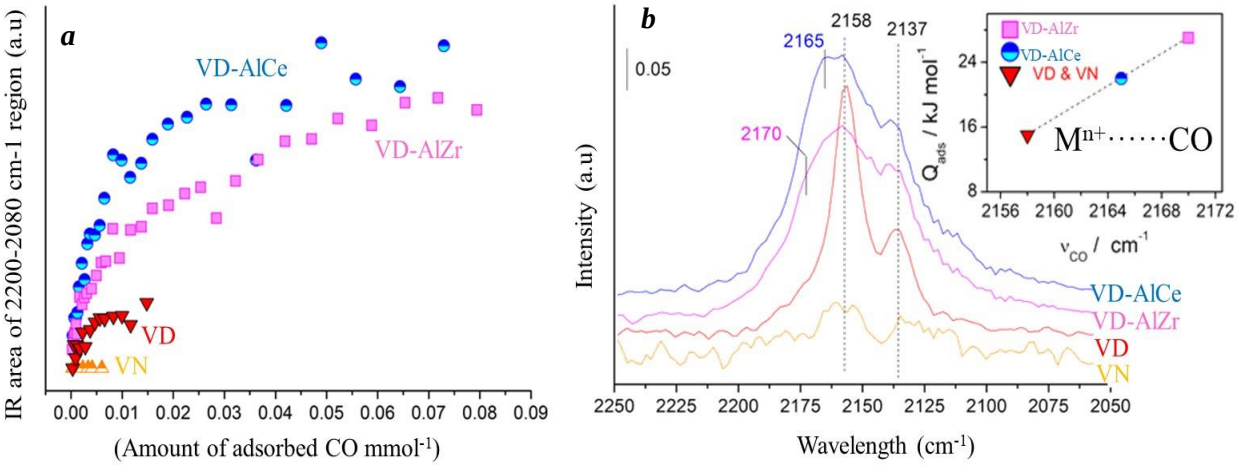

Figure 10. a) Relationship of the area with the amount of CO adsorbed. **b)** FTIR for the different solids after the adsorption of the maximum of CO in the ν region (CO). The inset shows the estimated adsorption of heat for the adsorption of CO in the different sites of Lewis acid cations.

While, following the incorporation of the AlZr and AlCe species, there is a notable increase in Lewis type acid strength (the bands observed at higher frequencies indicate greater interaction when Ce and Zr cations were added). The AlZr-modified solid presents a slight shift in the signal of adsorption of CO (2140 and 2170 cm^{-1}; ΔH= 24.5 $kJmol^{-1}$) compared to the AlCe (2137 and 2165 cm^{-1}; ΔH= 21.5 $kJmol^{-1}$), which can be associated with a slight increase in the Lewis type acid strength (discussed previously). This is associated to the different chemical species with which the CO interacts. In this way, they correspond to 2140, 2170, 2137 and 2165 cm^{-1} and are attributed to the Zr or Ce cations,

coordinated with CO respectively [68, 69], which, as observed by XPS are more likely to correspond to Zr^{4+} and Ce^{3+}. However, absorption near 2140 can also be attributed to species from pseudo-liquid CO species observed after CO saturation as reported [70]. Considering the Δν changes of the ν band (CO) for the different Zr and Ce cations, it can be concluded that the presence of small amounts of these cations increases the acidity of the materials. These results were previously discussed by NH_3-DRIFTS and NH_3-TPD, which indicates that, in effect, the solids incorporated with AlCe present the highest number of acid sites, while with Zr there is a slightly greater strength of acidic Lewis sites.

Catalytic activity

Fig. 11. illustrates the evolution of the intensities of the signals of 2-propanol, acetone, propylene, water and hydrogen respectively, during the dehydration-dehydrogenation of 2-propanol.

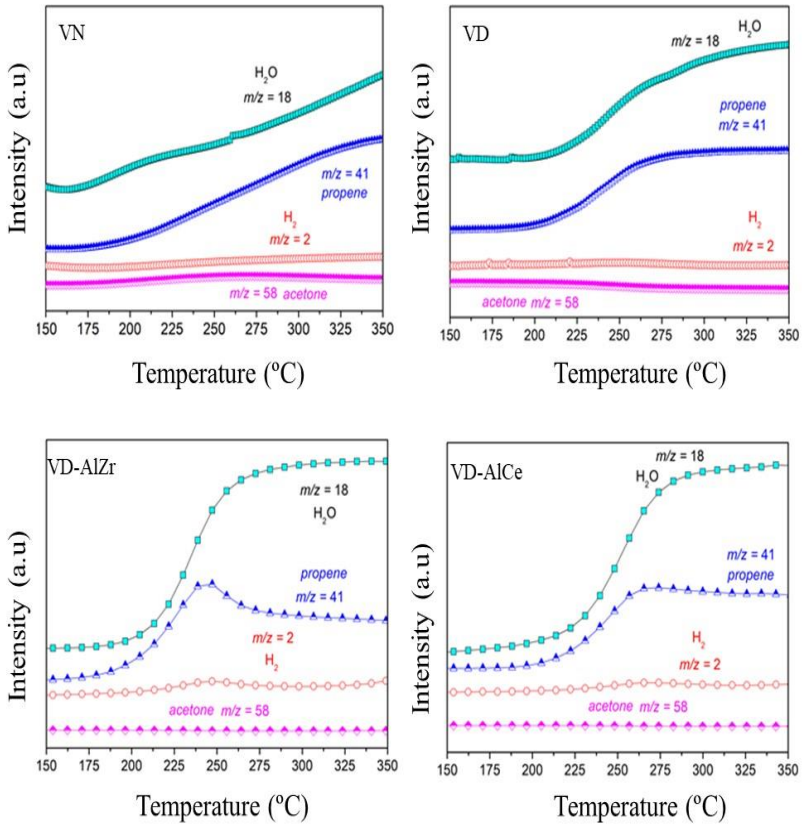

Figure 11. Monitoring of different species as a function of temperature and time during the dehydration-dehydrogenation of 2-propanol.

Dehydration generally competes with dehydrogenation, the proportion of each type of product obtained depends on the catalyst and the reaction conditions used, the selectivity of the catalyst being mainly governed by its acid-base properties where dehydration is generally caused in the acidic sites producing the corresponding alkene, while ketone is produced at the basic sites [20]. In this way, the production of propylene and the absence of acetone reveal the acidic properties of the solids, where 2-propanol is adsorbed in Brönsted type acid sites, thus generating a propoxy group, water and subsequently a hydrogen displacement to a neighboring oxygen site thus producing propylene according to Fig. 12. [71, 72].

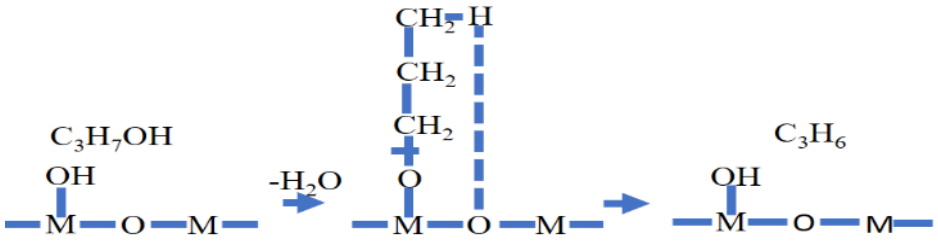

Figure 12. Production scheme of propylene from 2-propanol, adapted from [71, 72].

However, the mechanism can also be carried out in the presence of strong Brönsted or Lewis acid sites and occurs in two steps. In the first instance, the breakdown of the CO bond by the attack of the acid on the OH alcohol group, followed by the formation of an intermediate carbocation that transforms finally into propylene [73].

Thus, in the solids analyzed there are two facts that are worth mentioning: i) the low production of acetone due to the dehydrogenation of 2-propanol, indicating the absence of basic sites in the material and ii) the production mainly of propylene and hydrogen, the latter is produced at high temperatures and comes from the successive mechanism of the dehydration of 2-propanol to obtain molecular hydrogen, as mentioned above.

In this sense, the intensity ratio between the m/z signals of propylene are influenced by the presence of the cation (Fig. 13.), this proportion being higher with Ce, where a greater

amount of propylene and a smaller amount of hydrogen are produced compared to Zr. This effect indicates that on the surface of the Ce there are a greater number of Brönsted type acid sites. In addition, it is the Ce that presents more stable acidic sites, as indicated by the formation of propylene as a function of the temperature, while the Zr has a band of high acidity which decreases as the temperature increases.

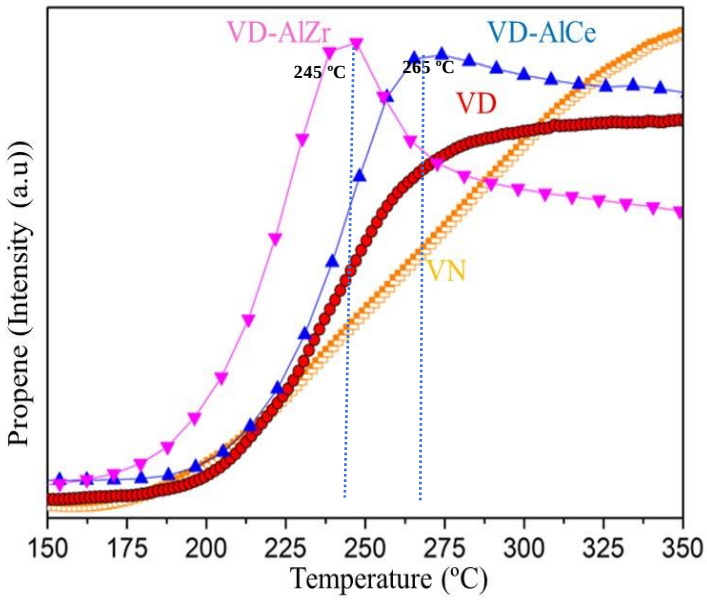

Figure 13. Intensity ratio between the m/z signals of propylene for different solids.

On the other hand, the shift towards lower temperatures in the propylene production observed for the solid with AlZr (245 ºC), compared to the solid with AlCe (265 ºC), is related to the acid strength of the Lewis acid sites. This concurs with the FTIR data in which it is seen that the AlZr has the greatest Lewis acid strength, as well as with the data in Table 1, where a lower B/L ratio is observed. Inferring that in this case there is a predilection for the dehydration of 2-propanol in strong Lewis acid sites, as has been reported in some cases in the literature [74].

As already mentioned, the hydroconversion of decane generates information regarding the acidity of the catalyst and, at the same time, allows for the evaluation of the catalytic behavior. This is a bifunctional reaction in which the acid site and the metallic site govern the mechanism [75]. However, in this work the use of the metallic function is omitted to

evaluate the variation of the acidity depending on the processes used for the modification of the vermiculite.

Fig. 14(a). shows the conversion profiles of the decane for the solids studied. As can be seen, the raw mineral achieves conversions of less than 10%, which can be attributed to the low specific surface area and the difficult access to acidic sites that this material presents. On the other hand, following the delamination an increase in the conversion is observed, close to 20%. This behavior is attributed to the acidic and textural properties already described.

The importance of the characteristics of the support and the textural and acidic properties in the catalytic activity, can be recognized by the changes in the conversion percentages observed when comparing with other types of previously reported materials [25, 34]. In all cases the conversion rates obtained from vermiculite are higher than with those obtained from other clay minerals without the incorporation of the metal phase.

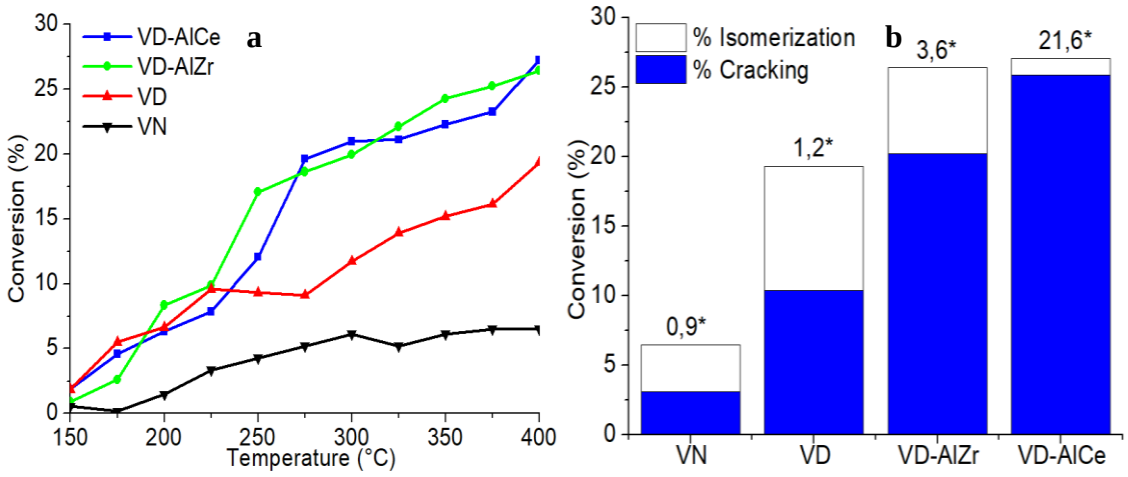

Figure 14. Decane activity as a function of the reaction temperature (a) and selectivity to isomerization and cracking products at 400 ºC (b). The error is ±3% in all cases [25, 27, 31].

*Ratio cracking products/isomerization products (C/I).

The results show a clear influence of the nature of the starting material on the activity and selectivity of the products obtained by demonstrating that, in the support, the number and strength of acid sites have an important role in the reaction mechanism. In fact, other

types of minerals lead mainly to isomerized products, vermiculite favors cracking products Fig. 14(b).

Isomerization is associated with the presence of a weak acidity, and/or a larger pore diameter. In contrast, cracking products are associated with strong acidity and a smaller pore diameter (2-10 nm) [25, 34, 76]. As has been reported [77], when the acid function is weak a lower hydrocracking activity is produced, whereas when the acid function is strong a high hydrocracking activity is generated as well as a low selectivity towards the isomers, due to the fact that there are a greater number of secondary reactions and a ratio is obtained between cracking products and isomerized products (C/I) > 1.

A comparison with a modified bentonite under the same conditions shows that each group of solids is specific for different reactions: bentonite is more selective for the hydroisomerization reaction, in all cases the ratio of cracking/isomerization products being (C/I) <1 [25], while in the vermiculite hydrocracking prevails, obtaining a C/I> 1 ratio as previously discussed.

On the other hand, a clear influence of the incorporated cation is observed, increasing the conversion up to nearly 30%, which is related to the acid properties already discussed evidencing the importance of the acidic characteristics of the support in the reaction.

Although the conversions for the VD-AlZr and VD-AlCe solids are similar, a knowledge of the reaction mechanism and a careful and rigorous study of the selectivity to cracking or isomerization products, become fundamental elements to have information related to the accessibility and strength of the acid sites during the hydroconversion reaction [25, 77].

In this context, as seen in Fig. 14(b), as the number and the acid strength of the solids increases, the number of isomers obtained decreases and the cracking reaction is favored. The C/I ratio increases in the following order: VN, VD, VD-AlZr and VD-AlCe, where

the solid VD-AlCe presents the greatest amount and strength of acidic sites, thus favoring the cracking reaction.

Considering that the determining step in the reaction mechanism is the average life-time of the carbocations and, consequently, the selectivity will be established by the residence time of said species, the conversion will be governed mainly by the acid character of the catalysts because their acid strength determines the degree of stability of the ions, the residence time on the surface and the type of reaction they will experience [78]. This allows for proposing a correlation between the catalytic activity and the total number of acid sites obtained by NH_3-TPD (Fig. 15.).

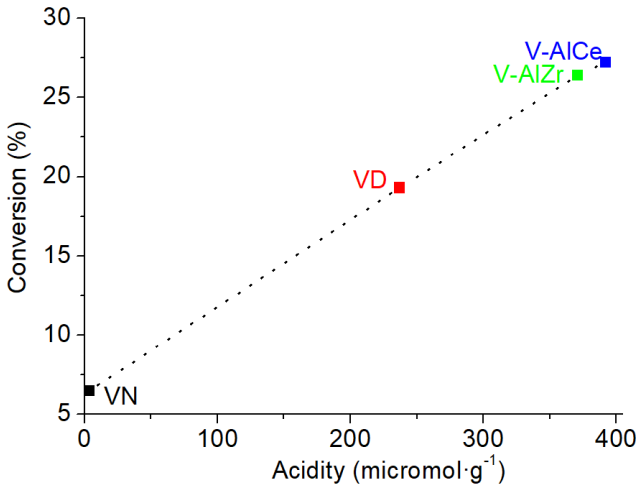

Figure 15. Correlation between the maximum decane conversion and total acidity, determined by NH_3-TPD.

It is observed that the solids present a linear tendency (R^2 of 0.999) between the acidity and the catalytic activity, where the reaction is favored by increasing the amount and strength of the acidic sites, indicating that the reference parameter of the activity in the decane conversion in materials is the concentration of acid sites, which are mainly Brönsted type as determined by DRIFTS.

In this way, the catalytic activity of each of the solids can be explained by the differences between the acidic properties where the incorporation of AlCe generates a greater number and greater strength of these sites, which is related to the capacity of Ce to stabilize Brönsted [55] type acid centers compared to Zr.

Conclusion

The acidity of the natural mineral for use as a catalytic support has been potentialized and modulated. The different classic characterization techniques used (XRD, IR, N_2 sortometry, SEM, NH_3-TPD NH_3-DRIFTS, XPS and the decane test and others less reported for clay minerals such as low temperature CO adsorption and dehydration/dehydrogenation of 2-propanol, have allowed for monitoring in the stages of synthesis and approaching the compression of the chemical processes that occur there.

The delamination process of vermiculite favorably modifies the textural properties and facilitates access to the intrinsic acid sites of the mineral. The insertion of AlZr and AlCe species allowed to significantly increase the acidity, generating solids with a wide range of acid property (from 3 to 392 μmol $NH_3 \cdot g^{-1}$). Obtaining solids with better textural and acidic properties and consequently a better catalytic performance compared to solids obtained from bentonite with the same modifications and reported in the literature.

The correlation between the number, the type and the acid strength with the catalytic behavior highlights the high potential of the intrinsic acidity of the vermiculite and its synergy with the delamination method and with the nature of the incorporated cation. Consequently, tools for controlled processes for the potentialization of the acidity of new starting raw vermiculite supports are generated, especially for reactions where acid sites with high strength are needed.

Acknowledgments

This research was carried out thanks to the financial support of Ecopetrol-Colciencias-Universidad de Antioquia-Universidad Nacional de Colombia, Contract 0405-2013. The project Hermes 41247 of the National University of Colombia (Bogotá) is also acknowledged. The authors gratefully acknowledge the cooperation of the Universidad

de Antioquia, especially to Andres Moreno and Natalia Suarez from the QUIREMA Group, for their valuable support in carrying out the NH_3-TPD analyzes.

Conflicts of interest

There are no conflicts to declare.

References

1. Moreno EL, Krishnaswamy Rajagopal (2009) Desafios da acidez na catálise em estado sólido. Quim Nov 32:538–542
2. Lv G, Wang C, Chi K, et al (2018) Effects of Pt site distributions on the catalytic performance of Pt/SAPO-11 for n-dodecane hydroisomerization. Catal Today 316:43–50.
3. Carlos L, Oliveira D De, Caetano R (2017) Hydroisomerization of n-hexadecane using Pt/alumina-Beta zeolite catalysts for producing renewable diesel with low pour point. Fuel 209:521–528.
4. Yadav GD (2005) Synergism of clay and heteropoly acids as nano-catalysts for the development of green processes with potential industrial applications. Catal Surv from Asia 9:117–137.
5. Wang L, Wang X, Yin J, Wang C (2016) Insights into the physicochemical characteristics from vermiculite to silica nanosheets. Appl Clay Sci 132–133:17–23.
6. Campos A, Gagea B, Moreno S, et al (2008) Decane hydroconversion with Al–Zr, Al–Hf, Al–Ce-pillared vermiculites. Appl Catal A Gen 345:112–118.
7. Tunega D, Lischka H (2003) Effect of the Si/Al ordering on structural parameters and the energetic stabilization of vermiculites - A theoretical study. Phys Chem Miner 30:517–522.
8. Cristiano D V, Campos AM, Molina R (2005) Charge reduction in a vermiculite by acid and hydrothermal methods: A comparative study. J Phys Chem B 109:19026–19033.
9. Zhang M, Li P, Zhu M, et al (2018) Ultralow-weight loading Ni catalyst supported on two-dimensional vermiculite for carbon monoxide methanation. Chinese J Chem Eng 26:1873–1878.
10. Pérez-Rodríguez JL, Carrera F, Poyato J, Pérez-Maqueda LA (2002) Sonication as a tool for preparing nanometric vermiculite particles. Nanotechnology 13:382–387.
11. Santos SSG, Silva HRM, Souza AG De, et al (2015) Acid-leached mixed vermiculites obtained by treatment with nitric acid. Appl Clay Sci 104:286–294.
12. Nguyen AN, Reinert L, Lévêque J, et al (2013) Preparation and characterization of micron and submicron-sized vermiculite powders by ultrasonic irradiation. Appl Clay Sci 72:9–17.
13. İşçi S (2017) Intercalation of vermiculite in presence of surfactants. Appl Clay Sci 146:7–13.
14. Chmielarz L, Rutkowska M, Jabłońska M, et al (2014) Acid-treated vermiculites as effective catalysts of high-temperature N_2O decomposition. Appl Clay Sci 101:237–245.
15. Hernández WY, Centeno MA, Odriozola JA, et al (2008) Acidity characterization of a titanium and sulfate modified vermiculite. Mater Res Bull 43:1630–1640.
16. Penkova A, Bobadilla LF, Romero-sarria F, et al (2014) Pyridine adsorption on NiSn/MgO – Al_2O_3: An FTIR spectroscopic study of surface acidity. Appl Surf Sci 317:241–251.
17. Sandoval-Díaz LE, González-Amaya JA, Trujillo CA (2015) General aspects of zeolite acidity characterization. Microporous Mesoporous Mater 215:229–243.
18. Webster CE, Drago RS, Zerner MC (1998) Molecular dimensions for adsorptives. J Am Chem Soc 120:5509–5516.
19. Cairon O, Chevreau T, Lavalley J. (1998) Bronsted acidity of extraframework debris in steamed Y zeolites from the FTIR study of CO adsorption. J Chem Soc 94:3039–3047.
20. Aramendía MA, Borau V, Jiménez C, et al (2000) Use of new tin orthophosphates as catalysts for the gas-phase dehydrogenation-dehydration of alcohols. Elsevier, pp 2141–2146
21. Sree SP, Dendooven J, Magusin PCMM, et al (2016) Hydroisomerization and hydrocracking activity enhancement of a hierarchical ZSM-5 zeolite cata. Catal Sci Technol 6:6177–6186.
22. Campos AM, Moreno S, Molina R (2008) Relationship between hydrothermal treatment parameters as a strategy to reduce layer charge in vermiculite, and its catalytic behavior. Catal Today 133–135:351–356.
23. Campos A, Gagea BC, Moreno S, et al (2007) Hydroisomerization of decane on Pt/Al, Ce-pillared vermiculites. In: Ruren Xu Jiesheng Chen and Wenfu Yan BT - Studies in Surface Science and Catalysis ZG (ed) From Zeolites to Porous MOF Materials. Elsevier, pp 1405–1410
24. Carriazo JG, Centeno MA, Odriozola JA, et al (2007) Effect of Fe and Ce on Al-pillared bentonite and their performance in catalytic oxidation reactions. Appl Catal A Gen 317:120–128.

25. Amaya J, Bobadilla L, Azancot L, et al (2020) Potentialization of bentonite properties as support in acid catalysts. Mater Res Bull 123:110728.
26. Ahmed A, Chaker Y, Belarbi EH, et al (2018) XRD and ATR/FTIR investigations of various montmorillonite clays modified by monocationic and dicationic imidazolium ionic liquids. J Mol Struct 1173:653–664.
27. Amaya J, Suarez N, Moreno A, et al (2019) Bifunctional catalysts supported on modified vermiculite for the hydroconversion of decane. Effect of the metal phase (Mo or W) and promoters (Ni or Co). Catal Today.
28. Buttersack C, Möllmer J, Hofmann J, Gläser R (2016) Determination of micropore volume and external surface of zeolites. Microporous Mesoporous Mater 236:63–70.
29. Liu D, Yuan P, Liu H, et al (2013) Quantitative characterization of the solid acidity of montmorillonite using combined FTIR and TPD based on the NH_3 adsorption system. Appl Clay Sci 80–81:407–412.
30. Lercher JA, Gründling C, Eder-Mirth G (1996) Infrared studies of the surface acidity of oxides and zeolites using adsorbed probe molecules. Catal Today 27:353–376
31. Castro A, Amaya J, Molina R, Moreno S (2019) Pillarization in concentrated media with solid Al and Al-Zr polymers to obtain acid catalysts. Catal Today.
32. Bobadilla LF, Muñoz-Murillo A, Laguna OH, et al (2019) Does shaping catalysts modify active phase sites? A comprehensive in situ FTIR spectroscopic study on the performance of a model Ru/Al_2O_3 catalyst for the CO methanation. Chem Eng J 357:248–257.
33. Domínguez MI, Sánchez M, Centeno MA, et al (2007) 2-Propanol oxidation over gold supported catalysts coated ceramic foams prepared from stainless steel wastes. J Mol Catal A Chem 277:145–154.
34. Torres-Luna JA, Moreno S, Molina R, Carriazo JG (2018) Hydroconversion of *n* -Decane over Ni–Mo Supported on Modified Halloysite Catalysts. Energy & Fuels 32:9782–9792.
35. Węgrzyn A, Stawiński W, Freitas O, et al (2018) Study of adsorptive materials obtained by wet fine milling and acid activation of vermiculite. Appl Clay Sci 155:37–49.
36. K. A. Carrado (2000) Synthetic organo-and polymer–clays : preparation, characterization, and materials applications. Appl Clay Sci 17:1–23
37. Shen F, Guo T, Bai C, et al (2018) Hydrolysis of cellulose with one-pot synthesized sulfonated carbonaceous solid acid. Fuel Process Technol 169:244–247.
38. Lee J, Hwang S, Seo JG, et al (2010) Production of middle distillate through hydrocracking of paraffin wax over Pd/SiO_2–Al_2O_3 catalysts. J Ind Eng Chem 16:790–794.
39. Awate S V, Waghmode SB, Agashe MS (2004) Synthesis, characterization and catalytic evaluation of zirconia-pillared montmorillonite for linear alkylation of benzene. Catal Commun 5:407–411.
40. Fuentes-Perujo D, Santamaría-González J, Mérida-Robles J, et al (2006) Evaluation of the acid properties of porous zirconium-doped and undoped silica materials. J Solid State Chem 179:2182–2189.
41. Mullins DR (2015) The surface chemistry of cerium oxide. Surf Sci Rep 70:42–85.
42. Tsud N, Cabala M (2009) A resonant photoemission applied to cerium oxide based nanocrystals 20 215706.
43. Hashimoto K, Matzuo K, Kominami H, Kera Y (1997) Cerium oxides incorporated into zeolite cavities and their reactivity. J Chem Soc - Faraday Trans 93:3729–3732.
44. Campos AM, Moreno S, Molina RA (2014) Characterization of Al-Zr, Al-Hf and Al-Ce-pillared vermiculites by X-ray photoelectron spectroscopy. Acad Colomb Cienc 38:401–408
45. Occelli ML (1988) Catal Today 2:339–355
46. Kaminski P, Ziolek M (2014) Surface and catalytic properties of Ce-, Zr-, Au-, Cu-modified SBA-15. J Catal 312:249–262.
47. Carriazo JG, Martínez LM, Odriozola JA, et al (2007) Gold supported on Fe, Ce, and Al pillared bentonites for CO oxidation reaction. Appl Catal B Environ 72:157–165.
48. Okada K, Arimitsu N, Kameshima Y, et al (2006) Solid acidity of 2:1 type clay minerals activated by selective leaching. Appl Clay Sci 31:185–193.
49. Dębek R, Ribeiro MFG, Fernandes A, Motak M (2015) Dehydration of methanol to dimethyl ether over modified vermiculites. Comptes Rendus Chim 18:1211–1222.
50. Heller-Kallai L (2001) Protonation-deprotonation of dioctahedral smectites. Appl Clay Sci 20:27–38.
51. Figueras F (1988) Pillared Clays as Catalysts. Catal Rev 30:457–499.
52. Moreno S, Kou RS, Molina R, Poncelet G (1999) Al-, Al,Zr-, and Zr-Pillared Montmorillonites and Saponites: Preparation, Characterization, and Catalytic Activity in Heptane Hydroconversion. J Catal 182:174–185.

53. Kooli F, Jones W (1997) Systematic Comparison of a Saponite Clay Pillared with Al and Zr Metal Oxides. Chem Mater 9:2913–2920
54. Ming-Yuan H, Zhonghui L, Enze M (1988) Acidic and hydrocarbon catalytic properties of pillared clay. Catal Today 2:321–338.
55. Fetter G, Salas P, Velazquez LA, Bosch P (2000) Ce-Al-pillared clays: Synthesis, characterization, and catalytic performance. Ind Eng Chem Res 39:1944–1949
56. Shimizu K, Nakamuro Y, Yamanaka R, et al (2006) Pillaring of high charge density synthetic micas (Na-4-mica and Na-3-mica) by intercalation of oxides nanoparticles. Microporous Mesoporous Mater 95:135–140.
57. Pálková H, Madejová J (2003) FTIR study of structural modifications of Li-montmorillonites. Solid State Phenom. 90–91:503–508
58. Zviagina BB, McCarty DK, Środoń J, Drits VA (2004) Interpretation of infrared spectra of dioctahedral smectites in the region of OH-stretching vibrations. Clays Clay Miner 52:399–410
59. Karakassides MA, Gournis D, Petridis D (1999) An infrared reflectance study of Si-O vibrations in thermally treated alkalisaturated montmorillonites. Clay Miner 34:429–438
60. Madejová J (2003) FTIR techniques in clay mineral studies. Vib Spectrosc 31:1–10
61. Basila MR (1962) An infrared study of a silica-alumina surface. J Phys Chem 66:2223–2228.
62. Morterra C, Magnacca G (1996) Surface characterization of modified aluminas. Part 5.-Surface acidity and basicity of CeO_2-Al_2O_3 systems. J Chem Soc Faraday Trans 92:5111–5116.
63. Morterra C, Bolis V, Magnacca G (1999) Surface characterization of modified aluminas. J Chem Soc Faraday Trans 92:1991–1999.
64. Saikia BJ, Parthasarathy G (2010) Fourier Transform Infrared Spectroscopic Characterization of Kaolinite from Assam and Meghalaya, Northeastern India. J Mod Phys 01:206–210.
65. Laubender E, Tanvir NB, Urban G, Yurchenko O (2016) Ceria-zirconia Mixed Oxide Prepared through a Microwave-assisted Synthesis for CO_2 Sensing in Low Power Work Function Sensors. Mater Today Proc 3:429–433.
66. Busca G, Lietti L, Ramis G, Berti F (1998) Chemical and mechanistic aspects of the selective catalytic reduction of NO_x by ammonia over oxide catalysts: A review. Appl Catal B Environ 18:1–36.
67. Petrini G, Spoto G, Padovan M, et al (2005) Silicalite characterization. 2. IR spectroscopy of the interaction of carbon monoxide with internal and external hydroxyl groups. J Phys Chem 96:4991–4997.
68. Hadjiivanov KI, Vayssilov GN (2002) Characterization of oxide surfaces and zeolites by carbon monoxide as an IR probe molecule. Adv Catal 47:307–511.
69. Claudio Morterra VB and GM (1996) Surface characterization of modified aluminas Part 4.t-Surface hydration and Lewis acidity of CeO_2-Al_2O_3 systems. Chem Soc Faraday Trans 92:1991–1999
70. Cairon O, Loustaunau A (2008) Adsorption of CO on NaY faujasite: A revisited FT-IR study. J Phys Chem C 112:18493–18501.
71. Arai, Hiromichi, Saito, Yasukazu, Yoneda Y (1968) Ethanol Dehydration on Alumina Catalysts. II. The Infrared study on Adsorption of Diethyl Ether over Alumina. J Catal 10:128–133
72. Shinohara Y, Nakajima T, Suzuki S (1999) A theoretical study of the dehydration and the dehydrogenation processes of alcohols on metal oxides using MOPAC. J Mol Struct THEOCHEM 460:231–244.
73. Ortiz-Islas E, López T, Navarrete J, et al (2005) High selectivity to isopropyl ether over sulfated titania in the isopropanol decomposition. J Mol Catal A Chem 228:345–350.
74. Gervasini A, Bellussi G, Fenyvesi J, Auroux A (1995) Microcalorimetric and catalytic studies of the acidic character of modified metal oxide surfaces. 1. Doping ions on alumina, magnesia, and silica. J Phys Chem
75. Zecevic J, Vanbutsele G, de Jong KP, Martens JA (2015) Nanoscale intimacy in bifunctional catalysts for selective conversion of hydrocarbons. Nature 528:245–248.
76. Martens JA, Verboekend D, Thomas K, et al (2013) Hydroisomerization and hydrocracking of linear and multibranched long model alkanes on hierarchical Pt/ZSM-22 zeolite. Catal Today 218–219:135–142.
77. Verheyen E, Jo C, Kurttepeli M, et al (2013) Molecular shape-selectivity of MFI zeolite nanosheets in n -decane isomerization and hydrocracking. J Catal 300:70–80.
78. Blomsma E, Martens JA, Jacobs PA (1996) Mechanisms of heptane isomerization on bifunctional Pd/H-beta zeolites. J Catal 159:323–331